SEMICONDUCTOR SIMULATIONS USING A COUPLED QUANTUM DRIFT-DIFFUSION SCHRÖDINGER-POISSON MODEL*

ASMA EL AYYADI† AND ANSGAR JÜNGEL†

Abstract. A coupled quantum drift-diffusion Schrödinger-Poisson model for stationary resonant tunneling simulations in one space dimension is proposed. In the ballistic quantum zone with the resonant quantum barriers, the Schrödinger equation is solved. Near the contacts, where collisional effects are assumed to be important, the quantum drift-diffusion model is employed. The quantum drift-diffusion model have been derived by a quantum moment method from a collisional Wigner equation by Degond et al. The derivation yields an $O(\hbar^4)$ approximation of the Wigner function which is used as the "alimentation function" in the mixed-state formula for the electron and current densities at the interface. The coupling of the two models is realized by assuming the continuity of the electron and current densities at the interface points. Current-voltage characteristics of a one-dimensional tunneling diode are numerically computed. The results are compared to those from the three models: quantum drift-diffusion equations, Schrödinger-Poisson system, and the coupled drift-diffusion Schrödinger-Poisson equations.

Key words. Schrödinger-Poisson system, quantum drift-diffusion model, quantum microscopic-macroscopic coupling, finite differences, resonant tunneling diode, hysteresis.

AMS subject classifications. 65M06, 82D37, 81V99.

1. Introduction.

Quantum effects in modern semiconductor devices are becoming of increasing importance in VLSI design. Devices which are based on quantum effects, like resonant tunneling diodes, can be used in logic applications [19] and are expected to improve the system performance of multi-GHz circuits in wireless communication systems [27]. Resonant tunneling diodes can be modeled by the Wigner equation [23] or the mixed-state Schrödinger equation [26]. However, the numerical computation of these equations is very expensive, even in one space dimension. Therefore, macroscopic quantum equations like quantum hydrodynamic or quantum drift-diffusion models have been devised [1, 15], whose numerical solution is much cheaper than solving microscopic models [18, 20, 22]. On the other hand, quantum diffusion models do not always give sufficiently physical accurate solutions [7].

In order to meet both demands (physical accuracy and numerical efficiency), *coupled microscopic-macroscopic models* can be employed. In these models, a microscopic quantum description is used in regions with dominant quantum effects and a macroscopic (fluid-type) model is employed in subregions in which collisional effects are expected to be dominant. In the case of a resonant tunneling diode, it has been proposed in [10] to use the stationary mixed-state Schrödinger equation in the (ballistic) channel region and the stationary drift-diffusion equations in the diffusion zones near the contacts. This approach has two advantages. First, the spatial domain in which the Schrödinger equation is solved can be reduced, thus also reducing the computational effort. Secondly, as the diffusion zone is assumed to be collision dominated, a diffusion approximation of the Wigner equation leads naturally to a coupling strategy between the quantum and classical equations.

*The authors acknowledge partial support from the Project "Hyperbolic and Kinetic Equations" of the European Union, grant HPRN-CT-2002-00282, the DAAD-Procope Program, and by the Deutsche Forschungsgemeinschaft (DFG), grant JU359/3 (Gerhard-Hess Award). The last author has been supported by the DFG, grant JU359/5 (Priority Program "Multi-scale Problems"). The authors thank Dr. Méhats (Toulouse) for very fruitful discussions.

†Fachbereich Mathematik und Informatik, Universität Mainz, Staudingerweg 9, 55099 Mainz, Germany; e-mail: {elayyadi,juengel}@mathematik.uni-mainz.de.

Similar coupling approaches have been proposed in the literature. A coupled kinetic-quantum model has been introduced in [4]. More precisely, a Boltzmann equation is solved in the classical zone and the stationary Schrödinger equation is computed in the quantum zone. At the interface between the classical and quantum zones, the boundary conditions for the Boltzmann equation depend on the reflection and transmission coefficients of the Schrödinger solution. The distribution function solving the Boltzmann equation is used as an "alimentation function" in the definition of the electron density in the quantum region. A time-dependent classical-quantum coupling strategy has been studied in [5]. Replacing the Boltzmann equation and the boundary conditions by the drift-diffusion model with interface conditions from a diffusion approximation leads to the already mentioned approach of [10]. The coupled drift-diffusion Schrödinger model has been recently extended to include collisions via a Pauli master equation [2]. A model in which a classical transport is assumed in the direction parallel to the electron gas and a quantum description in the transversal direction is analyzed in [6]. In [14] the quantum drift-diffusion model is used in the parallel direction instead of a classical transport description. For other coupling models we refer to, e.g., [3, 8].

In this paper we propose a slightly different approach compared to [10]. Instead of choosing a classical collision operator in the Boltzmann equation (from which the drift-diffusion model is derived) we start from the Wigner equation with a BGK collision operator. In [11] it has been shown that a diffusion approximation of the Wigner-BGK model leads to the so-called quantum drift-diffusion model (also called density-gradient model [1]),

$$\frac{\partial n}{\partial t} - \frac{1}{e}\mathrm{div}\, J = 0, \quad J = \mu_n \left(U_{\rm th}\nabla n - n\nabla(V + Q[n])\right),$$

where the variables are the electron density $n(x,t)$, the current density $J(x,t)$, and the electrostatic potential $V(x,t)$; the physical constants are the elementary charge e, the electron mobility $\mu_n = e\tau/m$, the effective electron mass m, the momentum relaxation time τ, and the thermal voltage $U_{\rm th}$. The expression

$$Q[n] = \frac{\hbar^2}{6em}\frac{\Delta\sqrt{n}}{\sqrt{n}}$$

denotes the quantum Bohm potential, where $\hbar$ is the reduced Planck constant. The fourth-order parabolic quantum drift-diffusion model has been analyzed and numerically solved in [22].

More precisely, we use the quantum drift-diffusion model in the diffusion region and the mixed-state Schrödinger equation in the ballistic zone. We restrict ourselves to the spatial one-dimensional stationary case in order to avoid complicate topological conditions on the device geometry. The advantage of our approach is that no (artificial) separation of the quantum and classical zones is necessary since a quantum description is employed in the whole device. The coupled model is solved self-consistently with the Poisson equation.

The coupling of the models is realized through connection conditions relating the macroscopic variables, namely the electron density and the current density, at the interface boundary points. We suppose that the particle and current densities are continuous across the interface. The current density computed from the Schrödinger equation depends on the statistics (or "alimentation function") used in the mixed-state formula. At the interface we assume that the statistics of the incoming particles

equals the $O(\hbar^4)$ approximation of the so-called quantum Maxwellian which is related to the quantum drift-diffusion model. This yields nonlinear boundary conditions for the macroscopic electron density and its derivatives.

The coupled model is numerically implemented using a finite-difference discretization and tested against a test case for a one-dimensional resonant tunneling diode taken from [26]. The numerical results show negative differential resistance in the current-voltage characteristic at room temperature, whereas the quantum drift-diffusion model in the whole domain is not able to reproduce these effects at room temperature (with the physical effective electron mass). Furthermore, hysteresis in the current-voltage curve can be observed in computations from our coupled model but not from the quantum drift-diffusion model. Compared to the numerical solution of the Schrödinger-Poisson system in the whole domain, the numerical effort of the coupled model is significantly reduced with comparable numerical solutions.

The paper is organized as follows. In the next section, the Schrödinger equation with open boundary conditions is presented and a sketch of the derivation of the quantum drift-diffusion model following [11] is given. Furthermore, the coupling of the two models is explained. Section 3 is concerned with the numerical discretization of the equations and the iteration procedure. Finally, some numerical results for a one-dimensional resonant tunneling diode are presented in section 4.

2. Presentation of the models. The semiconductor is assumed to occupy the interval $\Omega = (0, L)$ in which the ballistic quantum zone $\Omega_s = (x_1, x_2)$ is sandwiched between two quantum diffusion regions $\Omega_q = (0, x_1) \cup (x_2, L)$, and $0 < x_1 < x_2 < L$.

2.1. The Schrödinger model. We consider the Schrödinger equation in the interval (a, b), where $a = 0$, $b = L$ or $a = x_1$, $b = x_2$. In the first case we solve the Schrödinger equation in the whole semiconductor domain, in the latter case only in the ballistic quantum zone.

Let the electrostatic potential $V(x)$ be given and let $\widetilde{V} = V + V_{\text{ext}}$ be the sum of electrostatic and external potential (V_{ext} models, for instance, the double barriers). We solve the Schrödinger equation

$$-\frac{\hbar}{2}\frac{d}{dx}\left(\frac{1}{m}\frac{d\psi_p}{dx}\right) - e\widetilde{V}(x)\psi_p = E_p\psi_p, \quad x \in (a, b),\ p \in \mathbb{R}, \tag{2.1}$$

where $\hbar = h/2\pi$ is the reduced Planck constant, m the (generally position-dependent) effective mass of the electrons, e the elementary charge, and E_p is the total energy of the corresponding scattering state ψ_p, given by

$$E_p = \begin{cases} p^2/2m - e\widetilde{V}(a) & : \ p > 0 \\ p^2/2m - e\widetilde{V}(b) & : \ p < 0. \end{cases}$$

Here, $p = \hbar k$ is the crystal momentum and k the wave vector. We use the Lent-Kirkner boundary conditions for (2.1) [16, 24]

$$\hbar\psi_p'(a) + ip\psi_p(a) = 2ip, \quad \hbar\psi_p'(b) = ip_+(p)\psi_b(b) \quad \text{if } p > 0, \tag{2.2}$$

$$\hbar\psi_p'(b) - ip\psi_p(b) = -2ip, \quad \hbar\psi_p'(a) = -ip_-(p)\psi_p(a) \quad \text{if } p < 0, \tag{2.3}$$

where

$$p_\pm(p) = \sqrt{p^2 \pm 2em(\widetilde{V}(b) - \widetilde{V}(a))}. \tag{2.4}$$

These boundary conditions can be derived by solving the above Schrödinger equation in $\mathbb{R}$, extending the potential by the definitions $\widetilde{V}(x) = \widetilde{V}(a)$ for $x < a$ and $\widetilde{V}(x) = \widetilde{V}(b)$ for $x > b$. Then the solutions are plane waves in the intervals $(-\infty, a)$ and (b, ∞), i.e. for $p > 0$ [10]:

$$\begin{aligned} \psi_p(x) &= e^{ip(x-a)/\hbar} + r(p)e^{-ip(x-a)/\hbar} \qquad (x < a), \\ \psi_p(x) &= t(p)e^{ip_+(p)(x-b)/\hbar} \qquad (x > b), \end{aligned} \tag{2.5}$$

and for $p < 0$:

$$\begin{aligned} \psi_p(x) &= e^{-ip(x-b)/\hbar} + r(p)e^{ip(x-b)/\hbar} \qquad (x > b), \\ \psi_p(x) &= t(p)e^{-ip_-(p)(x-a)/\hbar} \qquad (x < a). \end{aligned} \tag{2.6}$$

The incoming wave is thus assumed to have amplitude one. The reflection and transmission amplitudes $r(p)$ and $t(p)$ are uniquely determined from the solution (see [10, p. 226]). By eliminating the unknowns $r(p)$ and $t(p)$, the boundary conditions (2.2)-(2.3) are obtained.

From the amplitudes $r(p)$ and $t(p)$ the reflection and transmission coefficients can be computed:

$$R(p) = |r(p)|^2, \quad T(p) = \frac{\mathrm{Re}(p_\pm(p))}{|p|}|t(p)|^2 \quad \text{if } \pm p > 0,$$

where "Re" denotes the real part of a complex number. It holds $R(p) + T(p) = 1$ for all $p \in \mathbb{R}$ and $T(p) = T(-p_+(p))$ for all $p > 0$ (reciprocity property).

We have to introduce some *macroscopic* quantities. The electron density $n_s(x)$ is defined by

$$n_s(x) = \int_{\mathbb{R}} g(p)|\psi_p|^2 dp, \tag{2.7}$$

where $g(p)$ is the statistics of the left reservoir if $p > 0$ and of the right reservoir if $p < 0$ (also called "alimentation function"), and the current density is given by

$$J_s(x) = \frac{e\hbar}{m}\int_{\mathbb{R}} g(p)\mathrm{Im}(\overline{\psi_p(x)}\psi_p'(x))dp, \tag{2.8}$$

where "Im" denotes the imaginary part of a complex number. In one space dimension the expression for the current density can be reformulated. Indeed, using (2.2)-(2.3) and (2.5)-(2.6), we obtain

$$\begin{aligned} \hbar\,\mathrm{Im}(\overline{\psi_p(a)}\psi_p'(a)) &= \mathrm{Im}(ip(1-|r(p)|)^2) = pT(p) \quad \text{for } p > 0, \\ \hbar\,\mathrm{Im}(\overline{\psi_p(a)}\psi_p'(a)) &= -\mathrm{Im}(ip_-(p)|t(p)|^2) = pT(p) \quad \text{for } p < -p_0, \end{aligned}$$

and $\hbar\,\mathrm{Im}(\overline{\psi_p(a)}\psi_p'(a)) = 0$ if $-p_0 < p \le 0$, where $p_0 = \mathrm{Re}\sqrt{2em(\widetilde{V}(b) - \widetilde{V}(a))}$. Therefore, since $J_s(x)$ is constant,

$$\begin{aligned} J_s(x) = J_s(a) &= \frac{e}{m}\int_0^\infty g(p)T(p)pdp + \frac{e}{m}\int_{-\infty}^{-p_0} g(p)T(p)pdp \\ &= \frac{e}{m}\int_0^\infty g(p)T(p)pdp + \frac{e}{m}\int_\infty^0 g(-p_+)T(-p_+)pdp \\ &= \frac{e}{m}\int_0^\infty (g(p) - g(-p_+))T(p)pdp, \end{aligned} \tag{2.9}$$

where we have used the substitution $p \mapsto -p_+(p)$ and the reciprocity property of $T(p)$.

The choice of the alimentation function $g(p)$ depends on the choice of a and b. If $a = 0$ and $b = L$, it is taken to be the Fermi-Dirac distribution:

$$g(p) = \frac{mk_BT_0}{2\pi^2\hbar^3} \ln\left\{1 + \exp\left[\frac{1}{k_BT_0}\left(-\frac{p^2}{2m} + E_F\right)\right]\right\},$$

where k_B is the Boltzmann constant, T_0 the lattice temperature, and E_F the Fermi energy computed from the charge-neutrality condition at the left or right reservoir boundary. This formula holds if the system is macroscopically large in its transversal dimensions (see [17, Ch. 9] or [25, Ch. 1.5.2.1]). In the case $a = x_1$ and $b = x_2$ we choose $g(p)$ as an approximation of the so-called quantum Maxwellian (see (2.16) and (2.11) below).

2.2. The quantum drift-diffusion model. In order to explain the coupling with the quantum drift-diffusion equations we need to review its derivation from a Wigner-BGK model as performed by Degond et al. [11, 12]. We start from the collisional Wigner equation in one space dimension

$$w_t + \frac{p}{m}w_x + \frac{e}{m}\theta[\widetilde{V}] = Q(w), \quad x, p \in \mathbb{R},\ t > 0, \tag{2.10}$$

where w_t, w_x denote the partial derivatives of w with respect to t and x, respectively, and $\theta[\widetilde{V}]$ is a pseudo-differential operator given by

$$(\theta[\widetilde{V}]w)(x,p,t) = \frac{i}{2\pi\hbar}\int_{\mathbb{R}^2}\left[\widetilde{V}\left(x + \frac{\hbar}{2m}\eta\right) - \widetilde{V}\left(x - \frac{\hbar}{2m}\eta\right)\right] \times w(x,p',t)e^{i\eta(p-p')/m}dp'd\eta.$$

(We do not indicate here the time-dependency of $\widetilde{V}$.) The collision operator is assumed to be of BGK type, i.e.

$$Q(w) = \frac{1}{\tau}(M[w] - w),$$

where τ is the relaxation time and $M[w]$ is the so-called quantum Maxwellian defined as minimizer of the quantum entropy, subject to the constraint of a given particle density [13]. In order to make this precise we introduce first the so-called relative quantum entropy.

Let W^{-1} be the inverse Wigner transform (or Weyl quantization):

$$(W^{-1}[w])\phi(x) = \frac{1}{2\pi\hbar}\int_{\mathbb{R}^2} w\left(\frac{x+y}{2}, p, t\right)\phi(y)e^{ip(x-y)/\hbar}dpdy \quad \text{for suitable } \phi(x).$$

The relative quantum entropy for the density matrix $\rho = W^{-1}[w]$ is defined as follows:

$$S(\rho) = \frac{1}{2\pi\hbar}\int_{\mathbb{R}^2} w\left(\mathrm{Ln}(w) - 1 + \frac{H}{k_BT_0}\right)dxdp,$$

where $H = |p|^2/2m - e\widetilde{V}(x)$ is the classical Hamiltonian, $\mathrm{Ln}(w) := W[\ln(W^{-1}[w])]$ is called the "quantum logarithm", and $\ln(f)$ is the usual operator logarithm. We wish to find, for given $n(x)$, the minimizer of

$$S(\rho^*) = \min\left\{S(\rho) : \frac{1}{2\pi\hbar}\int_{\mathbb{R}} W[\rho]dp = n(x) \quad \forall x\right\}.$$

The solution (if it exists) is $\rho_a = W^{-1}[w_a]$, where $w_a = \mathrm{Exp}(a(x) - H/k_BT_0)$ and $\mathrm{Exp}(f) := W[\exp(W^{-1}[f])]$ is called the "quantum exponential". The function $a(x)$ is such that $\int w_a(x,p)dp/2\pi\hbar = n(x)$. We call w_a a quantum Maxwellian. In other words, for given $w(x,p)$, we define $M[w]$ as the *quantum Maxwellian*

$$M[w] = \mathrm{Exp}\left(b(x) - \frac{|p|^2}{2mk_BT_0}\right)$$

such that $\int(M[w]-w)dp = 0$ and $b(x) = a(x) - e\widetilde{V}(x)/k_BT_0$. We assume that the integral constraint fixes the function $b(x)$ in a unique way [11].

The quantum drift-diffusion model is derived from (2.10) in the diffusion limit. For this, we introduce the scaling $t \to t/\delta$ and $Q(w) \to Q(w)/\delta$ which yields

$$\delta^2 w_t^\delta + \delta\left(\frac{p}{m}w_x^\delta + \frac{e}{m}\theta[\widetilde{V}]\right) = Q(w^\delta).$$

As $\delta \to 0$, the formal limit $w_0 = \lim_{\delta\to 0} w^\delta$ satisfies $Q(w_0) = 0$, hence $w_0 = M[w_0] = \mathrm{Exp}(b_0(x) - |p|^2/2mk_BT_0)$ for some function $b_0(x)$, and $n(x) = \int w_0(x,p)dp/2\pi\hbar$. In [11] has been shown by a Chapman-Enskog expansion method that n satisfies the equation

$$n_t - \frac{1}{e}J_x = 0, \quad J = \frac{\tau e k_BT_0}{m}nb_{0,x} - \frac{\tau e^2}{m}nV_x,$$

and n and b_0 are related by

$$n = \int_{\mathbb{R}} \mathrm{Exp}\left(b_0(x) - \frac{|p|^2}{2mk_BT_0}\right)\frac{dp}{2\pi\hbar}$$

(see [12, Lemma 6.5]). Furthermore, we can expand $w_0 = \mathrm{Exp}(b_0 - |p|^2/2mk_BT_0)$ and thus n and J in terms of $\hbar$.

LEMMA 2.1. *The following (formal) expansion holds for all $x, p \in \mathbb{R}$ up to order $O(\hbar^4)$:*

$$w_0(x,p) = A_0 e^{-p^2/2mk_BT_0} n\left[1 + \frac{\hbar^2}{12mk_BT_0}\left(1 - \frac{p^2}{mk_BT_0}\right)\left(\frac{(\sqrt{n})_{xx}}{\sqrt{n}} - \frac{(\sqrt{n})_x^2}{n}\right)\right], \tag{2.11}$$

where $A_0 = \sqrt{2\pi\hbar^2/mk_BT_0}$.

Notice that $(\sqrt{n})_{xx}/\sqrt{n} - (\sqrt{n})_x^2/n = (\log n)_{xx}$ but the formulation in (2.11) is more convenient later.

Proof. We use Lemma 5.6 of [11] to obtain

$$\begin{aligned} w_0(x,p) &= \exp\left(b_0 - \frac{p^2}{2mk_BT_0}\right) - \frac{\hbar^2}{8mk_BT_0}\exp\left(b_0 - \frac{p^2}{2mk_BT_0}\right) \\ &\quad \times \left[\left(-1 + \frac{p^2}{3mk_BT_0}\right)b_{0,xx} - \frac{1}{3}b_{0,x}^2\right] + O(\hbar^4). \end{aligned} \tag{2.12}$$

This gives

$$n(x) = \int_{\mathbb{R}} w_0(x,p)\frac{dp}{2\pi\hbar} = n_0(x) + \frac{\hbar^2}{24mk_BT_0}n_0(x)(2b_{0,xx} + b_{0,x}^2) + O(\hbar^4),$$

where $n_0 := \exp(b_0)/A_0$. Consequently, $n = n_0 + O(\hbar^2)$ and we can solve the above equation for n_0:

$$n_0 = n - \frac{\hbar^2}{24mk_BT_0} n(2b_{0,xx} + b_{0,x}^2) + O(\hbar^4).$$

Inserting this expression into (2.12) yields, after some computations,

$$w_0 = A_0 e^{-p^2/2mk_BT_0} n \left[1 + \frac{\hbar^2}{24mk_BT_0}\left(1 - \frac{p^2}{mk_BT_0}\right) b_{0,xx}\right] + O(\hbar^4).$$

Since

$$b_{0,xx} = 2\frac{(\sqrt{n})_{xx}}{\sqrt{n}} - \frac{n_x^2}{2n^2} + O(\hbar^2) = 2\frac{(\sqrt{n})_{xx}}{\sqrt{n}} - 2\frac{(\sqrt{n})_x^2}{n} + O(\hbar^2)$$

(see [11, sec. 5.3]), we conclude the assertion. □

In [11] it is shown that we can expand $n = n_q + O(\hbar^4)$, $J = J_q + O(\hbar^4)$, and n_q, J_q satisfy the so-called *quantum drift-diffusion equations*

$$n_{q,t} - \frac{1}{e} J_{q,x} = 0, \quad J_q = \frac{\tau e k_B T_0}{m} n_{q,x} - \frac{\tau e^2}{m} n_q (\widetilde{V} + Q[n_q])_x, \tag{2.13}$$

where

$$Q[n_q] = \frac{\hbar^2}{6em} \frac{(\sqrt{n_q})_{xx}}{\sqrt{n_q}}$$

is the so-called Bohm potential.

We can rewrite (2.13) by introducing the function $\rho = \sqrt{n_q}$ and the quantum quasi-Fermi potential

$$F = U_{\rm th} \ln n_q - \widetilde{V} - Q[n_q]$$

(with the thermal voltage $U_{\rm th} = k_BT_0/e$). Then the stationary version of (2.13) becomes

$$(\rho^2 F_x)_x = 0, \quad F = U_{\rm th} \ln \rho^2 - \widetilde{V} - \frac{\hbar^2}{6em} \frac{\rho_{xx}}{\rho}. \tag{2.14}$$

The current density equals $J_q = (\tau e^2/m)\rho^2 F_x = e\mu_n \rho^2 F_x$.

In order to specify boundary conditions for (2.14) we need to distinguish the two cases for the choice of a and b. Let first $a = 0$ and $b = L$. Then, following [22], we assume that the total space charge vanishes and that no quantum effects occur at the boundary (in the sense $(\sqrt{n_q})_{xx} = 0$). Thus

$$n_q(0) = n_D(0), \quad n_q(L) = n_D(L), \quad F(0) = 0, \quad F(L) = -V_a, \tag{2.15}$$

where V_a denotes the applied voltage. The case $a = x_1$ and $b = x_2$ is studied in the next subsection.

2.3. The coupled model. Let $a = x_1$ and $b = x_2$. We solve the Schrödinger equation (2.1) in (a, b) with boundary conditions (2.2)-(2.3) and the quantum drift-diffusion model (2.14) in the intervals $(0, x_1)$ and (x_2, L).

In order to compute the electron and current densities n_s and J_s, respectively (see (2.7) and (2.8)), we need to specify the alimentation function $g(p)$. We choose $g(p)$ as the $O(\hbar^4)$ approximation (2.11) of the quantum Maxwellian (see Lemma 2.1):

$$g(p) = w_0(a, p) \quad \text{if } p > 0, \quad g(p) = w_0(b, p) \quad \text{if } p < 0. \tag{2.16}$$

Although in general, w_0 does not need to be a nonnegative function, we observed in the numerical simulations that $w_0(a, p)$ and $w_0(b, p)$ are always positive. Another idea could be to choose the classical Maxwellian instead of the (approximation of the) quantum Maxwellian w_0 in (2.16). However, this choice did not lead to a converging algorithm (see section 3 for details on the discretization and the iterative procedure). A possible explanation could be that the use of the classical Maxwellian is not consistent with the use of the quantum drift-diffusion model.

The coupling of both models is realized through connection conditions relating the macroscopic unknowns (the electron density and the current density) at the two interface points x_1 and x_2. We assume that at the interface, the particle density and the current density is continuous, i.e.

$$n_q(x_1) = n_s(x_1), \quad n_q(x_2) = n_s(x_2), \quad J_q(x_1) = J_s(x_1), \quad J_q(x_2) = J_s(x_2).$$

Thus, the quantum drift-diffusion model is solved in $(0, x_1)$ with the four boundary conditions

$$n_q(0) = n_D(0), \quad F(0) = 0, \quad n_q(x_1) = n_s(x_1), \quad J_q(x_1) = J_s(x_1). \tag{2.17}$$

In the interval (x_2, L) we impose the boundary conditions

$$n_q(x_2) = n_s(x_2), \quad J_q(x_2) = J_s(x_2), \quad n_q(L) = n_D(L), \quad F(L) = -V_a. \tag{2.18}$$

The interface conditions for the current densities can be written in a form which is more convenient for the numerical computations. For this, we remark that we have from (2.16) and (2.9)

$$J_s(x_1) = \int_0^\infty w_0(a, p)T(p)pdp - \int_0^\infty w_0(b, -p_+(p))T(p)pdp$$

and J_s is constant in $[x_1, x_2]$. Inserting the above formula into $J_q(x_j) = J_s(x_j)$ $(j = 1, 2)$, some elementary computations give, up to order $O(\hbar^4)$,

$$\begin{aligned} J_q(x_2) = J_q(x_1) &= \sqrt{2\pi\theta}A_0\left(n_s(x_1) - e^{-\delta V/2\theta}n_s(x_2)\right)I_1 \\ &\quad + \sqrt{2\pi\theta}\frac{\hbar^2 A_0}{12}n_s(x_1)\left(\frac{\rho_{xx}}{\rho} - \frac{\rho_x^2}{\rho^2}\right)_{x=x_1}(\theta I_1 - I_2) \\ &\quad + \sqrt{2\pi\theta}\frac{\hbar^2 A_0}{12}n_s(x_2)\left(\frac{\rho_{xx}}{\rho} - \frac{\rho_x^2}{\rho^2}\right)_{x=x_2}e^{-\delta V/2\theta}((\theta - \delta V)I_1 - I_2), \end{aligned}$$

where $\rho = \sqrt{n_q}$, $\theta = mk_BT_0$, $\delta V = 2em(V(x_2) - V(x_1))$, and

$$I_1 = \frac{1}{\sqrt{2\pi\theta}}\int_0^\infty pT(p)e^{-p^2/2\theta}dp, \quad I_2 = \frac{1}{\sqrt{2\pi\theta}}\int_0^\infty p^3T(p)e^{-p^2/2\theta}dp.$$

For the numerical computations we replace the Bohm potential term ρ_{xx}/ρ by the expression (2.14) in order to avoid the computation of the second derivatives of ρ. This gives two nonlinear boundary conditions for the quantum quasi-Fermi potential F:

$$n_s(x_j)F_x(x_j) = f(F(x_1), F(x_2), \rho_x(x_1), \rho_x(x_2)), \quad j = 1, 2,$$

where

$$\begin{aligned}
&f(F(x_1), F(x_2), \rho_x(x_1), \rho_x(x_2)) = \sqrt{2\pi\theta}A_0 I_1 \left(n_s(x_1) - e^{-\delta V/2\theta} n_s(x_2)\right) \\
&+ \frac{em}{2}\sqrt{2\pi\theta}A_0(\theta I_1 - I_2)n_s(x_1)\left(F(x_1) - U_{\rm th}\ln n_s(x_1) + \widetilde{V}(x_1) + \frac{\hbar^2}{6em}\frac{\rho_x^2(x_1)}{n_s(x_1)}\right) \\
&+ \frac{em}{2}\sqrt{2\pi\theta}A_0 e^{-\delta V/2\theta}((\theta - \delta V)I_1 - I_2)n_s(x_2) \\
&\times \left(F(x_2) - U_{\rm th}\ln n_s(x_2) + \widetilde{V}(x_2) + \frac{\hbar^2}{6em}\frac{\rho_x^2(x_2)}{n_s(x_2)}\right).
\end{aligned}$$

Finally, the electric potential is self-consistently coupled through the Poisson equation

$$\frac{d}{dx}\left(\varepsilon_s\frac{dV}{dx}\right) = e(n - n_D(x)), \quad x \in (0, L),$$

where ε_s is the semiconductor permittivity and the particle density $n(x)$ is given by

$$n(x) = \begin{cases} n_q(x) & : x \in (0, x_1) \cup (x_2, L) \\ n_s(x) & : x \in (x_1, x_2). \end{cases} \tag{2.19}$$

3. Numerical discretization. We discretize the equations by introducing a uniform mesh $\xi_k = k\triangle x$, $\triangle x > 0$, $k = 0, \ldots, K$, and $L = K\triangle x$.

The Schrödinger equation is solved by central finite differences as in [10]. For the convenience of the reader we recall the discretization scheme. We assume that the effective mass is constant in $[x_1, x_2]$ since we wish to compare our results with those from the literature, e.g. [7, 26]. Moreover, a space-dependent effective electron mass leads to quite complicate quantum drift-diffusion models whose numerical solution is delicate [28]. The Schrödinger equation (2.1) with boundary conditions (2.2) for $p > 0$ (the case $p < 0$ can be treated analogously) can be equivalently rewritten as

$$y'' = -\frac{2m}{\hbar^2}(E_p + e\widetilde{V})y \quad \text{in } (x_1, x_2), \quad y(x_2) = 1, \quad y'(x_2) = \frac{i}{\hbar}p_+(p), \tag{3.1}$$

where $p_+(p)$ is defined in (2.4) and y and ψ_p are related by

$$\psi_p(x) = \frac{2ipy(x)}{\hbar y'(x_1) + ipy(x_1)}.$$

With the approximations $y_k \approx y(\xi_k)$ and $\widetilde{V}_k \approx \widetilde{V}(\xi_k) = V_{\rm ext}(\xi_k) + V(\xi_k)$ the discrete problem is

$$\frac{1}{(\triangle x)^2}(y_{k+1} - 2y_k + y_{k-1}) = -\frac{2m}{\hbar^2}(E_p + e\widetilde{V}_k)y_k.$$

This problem is solved as in [10] by Stoermer's method, i.e. writing

$$z_k = \frac{y_{k+1}-y_k}{\triangle x} \quad (k=0,\ldots,K-1), \quad z_K = y'(x_2) - \frac{m}{\hbar^2}(E_p + e\widetilde{V}(x_2))y(x_2)$$

and noticing that z_K is known in view of (3.1), the iteration reads:

$$\begin{aligned} z_k &= z_{k+1} - \frac{m}{\hbar^2}\triangle x(E_p + e\widetilde{V}_{k-1})y_{k-1}, \\ y_k &= y_{k+1} - \triangle x z_k, \\ y_0' &= y'(x_1) = z_1 - \frac{m}{\hbar^2}\triangle x(E_p + e\widetilde{V}_0)y_0, \end{aligned}$$

which allows to calculate z_k and y_k recursively. The algorithm is vectorized and implemented in MATLAB.

The quantum drift-diffusion model (2.14) is approximated by central finite differences as in [22]. The proposed scheme has been proved to be positivity preserving, i.e., the discrete electron density is positive (see [21, 22] for details). Let ρ_k and F_k be approximations of $\rho(\xi_k)$ and $F(\xi_k)$, respectively. Then the discrete problem corresponding to (2.14) is

$$\frac{1}{(\triangle x)^2}\left(\rho_{k+1/2}^2 F_{k+1} - (\rho_{k+1/2}+\rho_{k-1/2})F_k + \rho_{k-1/2}^2 F_{k-1}\right) = 0, \tag{3.2}$$

$$F_k = U_{\rm th}\ln\rho_k^2 - \widetilde{V}_k - \frac{\hbar^2}{6em(\triangle x)^2}\frac{\rho_{k+1}-2\rho_k+\rho_{k-1}}{\rho_k}, \tag{3.3}$$

where $\rho_{k\pm1/2} = (\rho_k+\rho_{k\pm1})/2$.

Finally, the discrete Poisson equation for $V_k \approx V(\xi_k)$ reads as follows:

$$\frac{\varepsilon_s}{(\triangle x)^2}(V_{k+1}-2V_k+V_{k-1}) = e(n_k - n_D(\xi_k)) \quad (k=1,\ldots,K-1), \quad V_0=0, \quad V_K = U,$$

where we have assumed a constant semiconductor permittivity ε_s, and the electron density is either given by (2.7) (discretized by a standard quadrature formulae) in the interval $[x_1,x_2]$ or by ρ_k^2 otherwise.

We describe now the iterative procedures for the various models. We use a fixed-point strategy to solve the Schrödinger-Poisson system in $(0,L)$ (i.e. $a=0$ and $b=L$). More precisely, we choose the electrostatic potential $V^{(0)}$ of the thermal equilibrium state as an initial guess. This potential is the (discrete) solution of the Poisson equation in which the electron density is replaced by the Thomas-Fermi approximation:

$$\varepsilon_s\frac{d^2V}{dx^2} = e\left(N_c F_{1/2}\left(\frac{\mu-\widetilde{V}}{k_BT_0}\right) - n_D(x)\right) \quad \text{in } (0,L), \quad V(0)=V(L)=0.$$

Here, $N_c = 2(mk_BT_0/2\pi\hbar^2)^{3/2}$ is the effective density of states and $F_{1/2}$ is the Fermi integral of order $1/2$ [17, Ch. 9]. The chemical potential μ is a constant in thermal equilibrium and computed from the nonlinear equation $n_D(0) = n(0) = F_{1/2}(\mu/k_BT_0)$ (where we assumed charge neutrality). With this initial potential we solve the discrete Schrödinger problem to obtain the (discrete) scattering states which allow to compute the discrete electron density from (2.7) and the discrete current density from (2.8). Finally, the update of the electric potential can be computed from the Poisson equation written in the Gummel formulation (see (3.8) in [10])

$$\varepsilon_s\frac{d^2V^{(j+1)}}{dx^2} + e(V^{(j+1)}-V^{(j)})n^{(j)} = e(n^{(j)}-n_D(x)).$$

The solution of the Schrödinger eigen value problem is the most costly part of the iteration. Indeed, we use a uniform grid of 10,000 values for p with grid size $\triangle p = 0.0005\sqrt{mk_BT_0}$. An adaptive mesh size strategy has been proposed for the Schrödinger-Poisson system in the whole domain in [7], but we observed that the adaptive algorithm did not converge for the coupled model.

Another idea to reduce the computing time is to choose different mesh sizes $\triangle x_q$ in the collisional zone and $\triangle x_s$ in the ballistic zone. However, it turned out in our numerical experiments that the computing time is minimized when using the same mesh size in both zones, i.e. $\triangle x = \triangle x_s = \triangle x_q$. We have used $\triangle x = 0.25\,\mathrm{nm}$ (540 grid points).

The quantum drift-diffusion model in the whole interval $(0, L)$ is solved by Newton's method. The initial guess is chosen to be the potential in thermal equilibrium with $V_a = 0$ (see (2.15)). In thermal equilibrium the quantum quasi-Fermi potential F is constant and, in view of the boundary conditions (2.15), the constant is zero. Then the thermal equilibrium potential is computed by a fixed-point scheme, i.e., we solve first the discrete equation

$$\frac{\hbar^2}{6em(\triangle x)^2}(\rho_{k+1} - 2\rho_k + \rho_{k-1}) = \rho_k(U_{\mathrm{th}} \ln \rho_k^2 - \widetilde{V}_k), \quad \rho_0 = n_D(0), \quad \rho_K = n_D(L),$$

employing Newton's method and then the linear Poisson equation with homogeneous boundary conditions.

In the case $a = x_1$ and $b = x_2$ we use again a fixed-point-type iteration. More precisely, let an initial guess for the potential be given (namely, the thermal equilibrium potential of the quantum drift-diffusion model). Then compute the scattering states from the discrete Schrödinger equation. The electron and current densities are calculated according to (2.7) and (2.8) where the approximation (2.16) is employed. The quantum drift-diffusion system is solved by Newton's method according to (3.2)-(3.3) using the boundary conditions (2.17) and (2.18), respectively. Finally, an update for the electric potential is obtained through the solution of the Poisson equation using the definition (2.19).

For all model we use the continuation method in the applied voltage, i.e., with the solution for the applied voltage U as an initial guess, we solve the problem applying the potential $V_a = U + \triangle U$ and use this solution again as initial guess for the next applied voltage. For the computations of the next section, we choose $\triangle U = 0.005\,\mathrm{V}$.

4. Numerical results. In this section we simulate a simple one-dimensional resonant tunneling diode. We choose the same geometry and data as in [26] (essentially taken from [23]). The tunneling diode consists of highly doped GaAs regions near the contacts and a lightly doped middle region of 35 nm length (see Figure 4.1). The middle region contains a quantum well of 5 nm length sandwiched between two 5 nm AlGaAs barriers. The double barrier heterostructure is placed between two 10 nm GaAs spacer layer with a doping of $5 \cdot 10^{15}\ \mathrm{cm}^{-3}$. These spacers are enclosed by two layers of 50 nm length and with doping $10^{18}\,\mathrm{cm}^{-3}$. The total length is thus 135 nm. The double barrier height is 0.3 eV. The physical effect of the barriers is a shift in the quasi-Fermi potential level which we model by an additional step function V_{ext} added to the electrostatic potential. The physical constants are chosen as in [26] and are summarized in Table 4.1.

First we present the current-voltage characteristics of the above tunneling diode for four different model equations: the Schrödinger-Poisson (SP) model in the whole interval, the coupled drift-diffusion Schrödinger-Poisson (DD-SP) model of [10], the

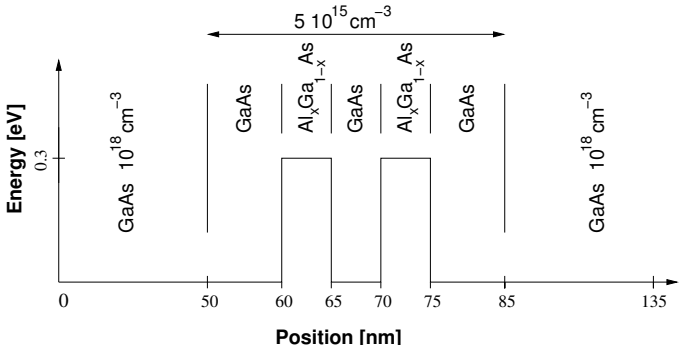

FIG. 4.1. *Geometry of the resonant tunneling diode and external potential $V_{\rm ext}$ modeling the double barriers.*

Parameter	physical meaning	numerical value
m	electron mass	$0.067 \cdot 9.11 \cdot 10^{-31}\,\mathrm{kg}$
T	lattice temperature	$300\,\mathrm{K}$
ε_s	semiconductor permittivity	$11.44 \cdot 8.85 \cdot 10^{-12}\,\mathrm{As/Vm}$
τ	relaxation time	$10^{-12}\,\mathrm{s}$
k_B	Boltzmann constant	$1.36 \cdot 10^{-23}\,\mathrm{J/K}$
$\hbar$	reduced Boltzmann constant	$1.055 \cdot 10^{-34}\,\mathrm{Js}$

TABLE 4.1
Physical parameters and their numerical values.

coupled quantum drift-diffusion Schrödinger-Poisson (QDD-SP) model presented in this paper, and the quantum drift-diffusion (QDD) model in the whole interval. We refer to [2, 10] for a description of the DD-SP model and its numerical discretization. Figure 4.2 displays the current-voltage curves for the first three models. In all these models, a region of negative differential resistance (NDR), in which the current is decreasing, can be observed. The valley current appears at approximately the same voltage but the voltage at which the peak current is observed is slightly different in the models. Moreover, the peak-to-valley ratio in the QDD-SP model is smaller than in the SP model. This comes probably from the fact that there are no collisions modeled in the SP system. In [2] a decrease of the peak-to-valley ratio has also been observed in simulations from the collisional DD-SP model (compared to the ballistic DD-SP model). The electron density and the electrostatic potential at applied voltage $V_a = 0.25\,\mathrm{V}$ are presented in Figures 4.3 and 4.4, respectively. The results obtained here compare well with those of [2] and [26], where the coupled DD-SP model and the SP model, respectively, were solved.

The current-voltage curve computed from the QDD model does not show any NDR region (Figure 4.5). In fact, the QDD model is too diffusive, thus distroying the quantum resonance behavior (at least at large temperatures). It is known that a non-monotone behavior of the current-voltage characteristic from the QDD model can be obtained by fitting the effective electron mass. Notice that the values for the current density are overestimated compared to the other models.

For comparison, the current-voltage characteristics for the SP, QDD-SP, and DD-SP models at $T = 77\,\mathrm{K}$ are displayed in Figure 4.6. The current-voltage curves of the two coupled models differ significantly from the curve computed from the SP model.

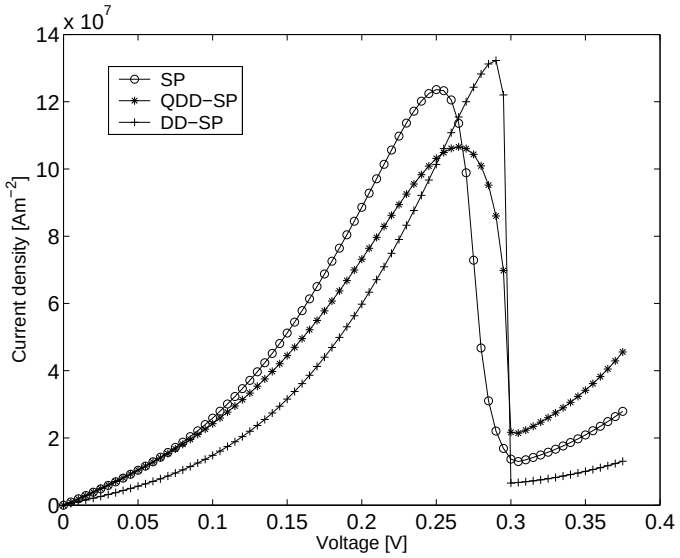

FIG. 4.2. *Current-voltage characteristics for a resonant tunneling diode using the SP, QDD-SP, and DD-SP models.*

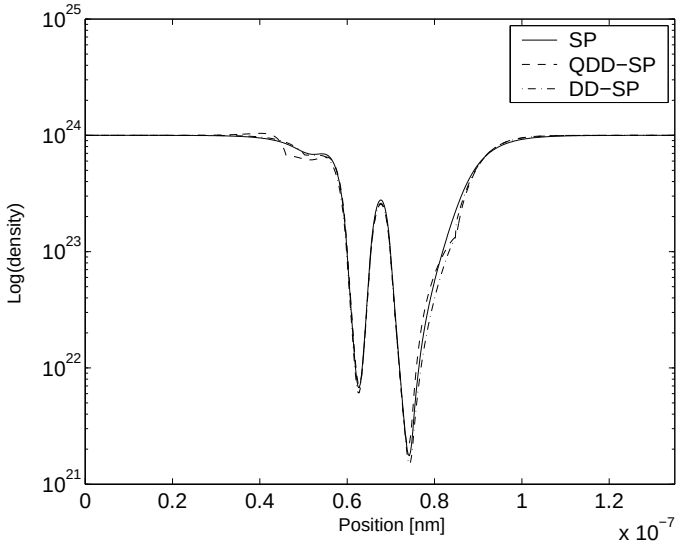

FIG. 4.3. *Electron densities at applied voltage $V_a = 0.25$ V from the SP, QDD-SP, and DD-SP models.*

This can be understood by the fact that at this low temperature, collisional effects are expected to be less important such that the use of diffusion models is questionable. However, the peak current from the QDD-SP model coincides with the peak current from the SP model, whereas the DD-SP model overestimates the peak current.

In [10] it has been observed that the current-voltage values depend quite sensitively on the position of the left interface point $a = x_1$ but the influence of the position of the right interface $b = x_2$ is very small. This observation holds true also

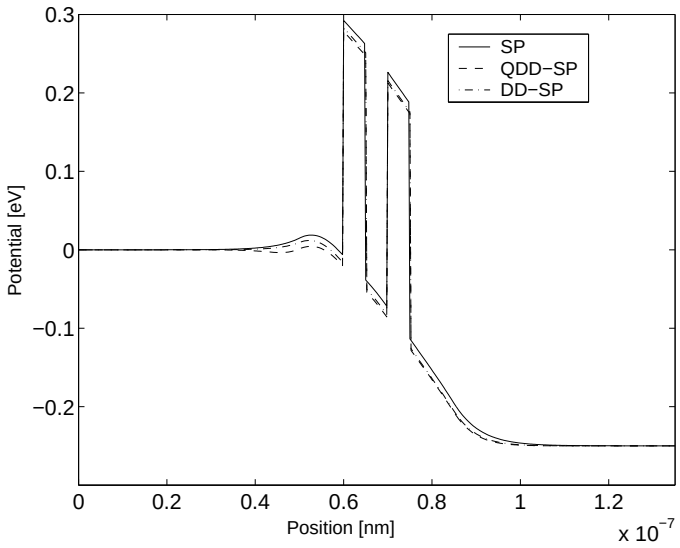

FIG. 4.4. *Potential profiles at applied voltage $V_a = 0.25$ V from the SP, QDD-SP, and DD-SP models.*

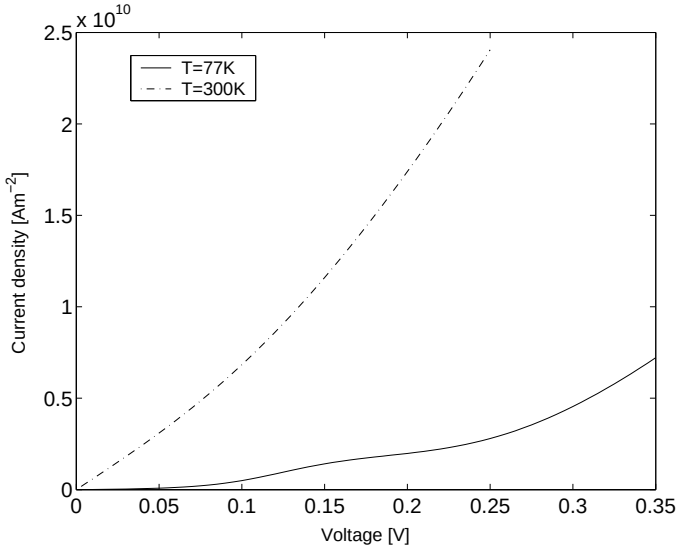

FIG. 4.5. *Current-voltage characteristics for a resonant tunneling diode using the QDD model for two different lattice temperatures.*

for the QDD-SP model (Figures 4.7 and 4.8). When the left interface is too close to the double barrier, the potential in the quantum region cannot reproduce the correct quantum resonances. It is argued in [10] that the insensitivity of the choice of the right interface position comes from the fact that the electrons crossing the double barriers have high energy and can be described equally well by a classical or a quantum model.

We have also investigated the effect of the relaxation time τ on the current-voltage

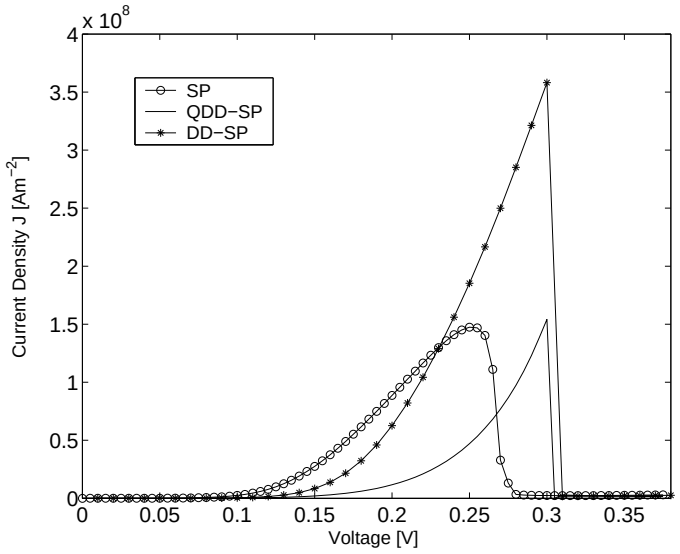

FIG. 4.6. *Current-voltage characteristics for a resonant tunneling diode using the SP, QDD-SP, and DD-SP models at temperature $T = 77\ K$.*

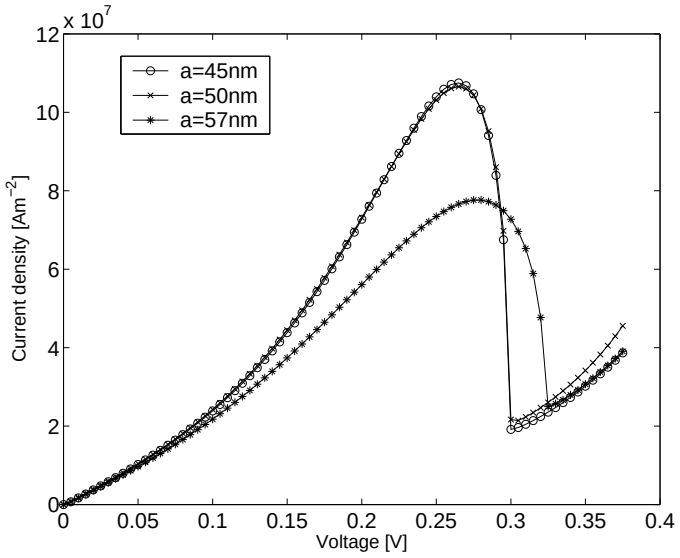

FIG. 4.7. *Influence of changes of the interface $a = x_1$ on the current-voltage characteristics using the QDD-SP model.*

curve. Figure 4.9 shows that the results are insensitive of the choice of τ. This holds true also in the ballistic DD-SP model of [10] (see Figure 4.10). In the collisional DD-SP model of [2], however, the characteristic is very sensitive with respect to τ. This seems to come from the collision events in the quantum region modeled by the Pauli master equation. Notice that in the coupled DD-SP and QDD-SP models, no collisions are taken into account in the microscopic quantum region.

It is well known that the current-voltage curve of a tunneling diode exhibits

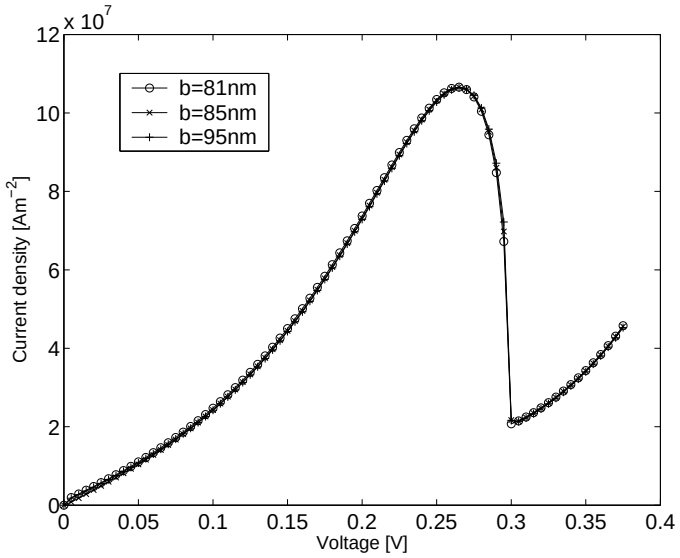

FIG. 4.8. *Influence of changes of the interface $b = x_2$ on the current-voltage characteristics using the QDD-SP model.*

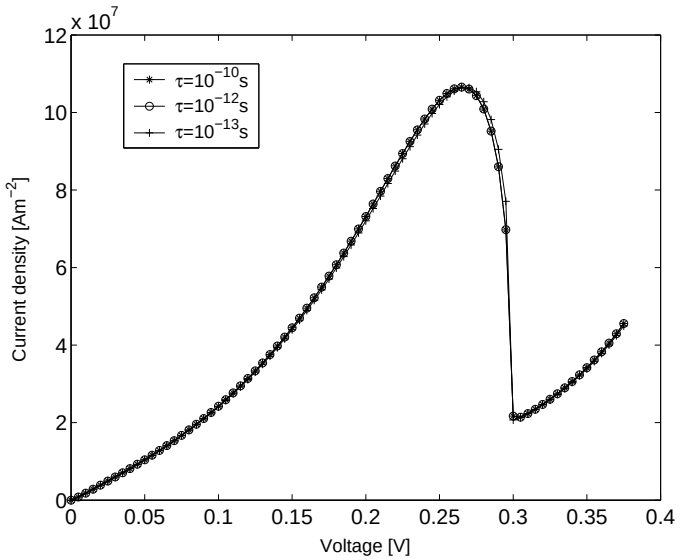

FIG. 4.9. *Influence of the relaxation time on the current-voltage characteristic using the QDD-SP model.*

hysteresis probably resulting from storage effects of the charges in the quantum well [23]. Hysteresis can be found in simulations from the Wigner-Poisson model [23] or from the quantum hydrodynamic equations [9]. It cannot be observed in simulations from the QDD model. However, employing the coupled QDD-SP model, the current-voltage characteristic shows hysteresis (Figure 4.11). We notice that also with the DD-SP model, hysteresis effects can be found (Figure 4.12).

Finally, Table 4.2 displays the CPU times (for a 2.4 GHz Pentium 4 processor)

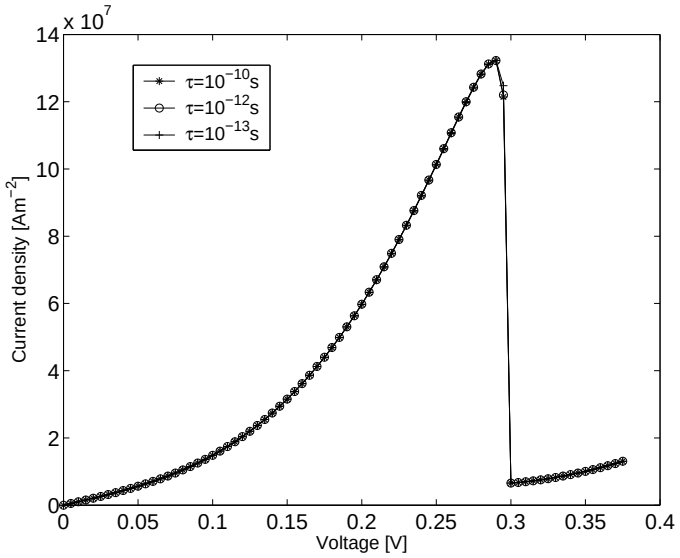

FIG. 4.10. *Influence of the relaxation time on the current-voltage characteristic using the DD-SP model.*

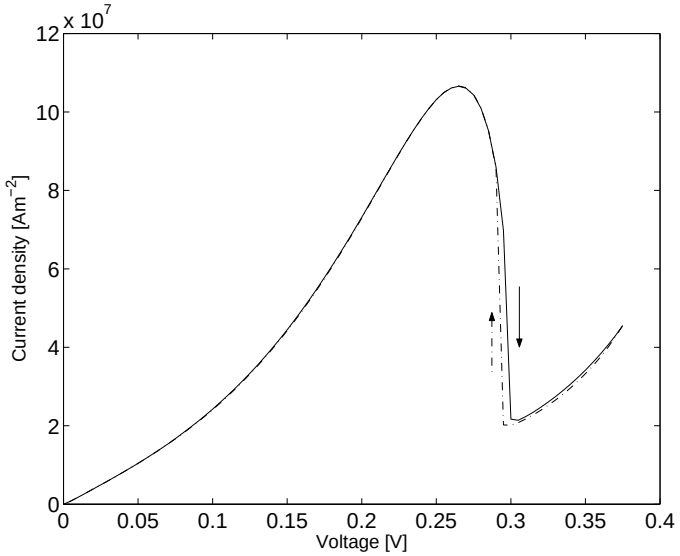

FIG. 4.11. *Hysteresis in the current-voltage characteristic using the QDD-SP model.*

needed to compute the current-voltage characteristic in various voltage ranges for the SP, QDD-SP and DD-SP models. All algorithms are vectorized in the same way such that the CPU times are comparable. The CPU time needed to calculate the current-voltage curve with the QDD model is of the order of a few seconds only; however, the numerical results are not satisfying. The QDD-SP model needs only about half of the CPU time compared to the SP model. This shows that the coupled model allows to reduce significantly the computing time compared to the full SP model.

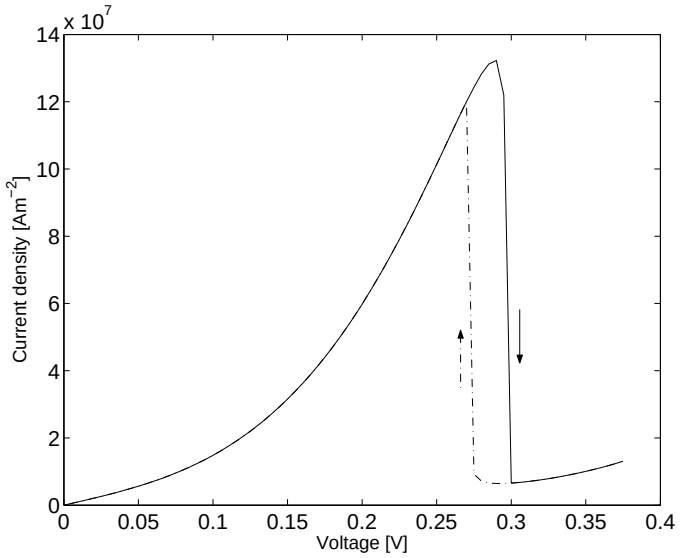

FIG. 4.12. *Hysteresis in the current-voltage characteristic using the DD-SP model.*

model	[0 0.25eV]	[0.25eV 0.3eV]	[0.3eV 0.375eV]	[0 0.375eV]
SP	5776 s	1255 s	1371 s	8402 s
QDD-SP	2305 s	570 s	629 s	3504 s
DD-SP	695 s	187 s	168 s	1050 s

TABLE 4.2

CPU times needed to compute the current-voltage characteristic in the indicated voltage ranges, using different models.

The DD-SP model is even faster; the reduction factor is about 8 compared to the SP model and about 3 compared to the QDD-SP model. The latter model is faster since the current density in the drift-diffusion region can be computed by an analytic expression [2, formulae (16)], whereas the current density of the QDD-SP model is a result of the solution of the QDD model. However, the QDD-SP model has the advantage that there is a quantum description in the whole semiconductor device, avoiding any artificial separation of classical and quantum zones.

REFERENCES

[1] M. Ancona and G. Iafrate, *Quantum correction to the equation of state of an electron gas in a semiconductor*, *Phys. Rev. B* **39** (1989), 9536-9540.

[2] M. Baro, N. Ben Abdallah, P. Degond, and A. El Ayyadi. A 1D coupled Schrödinger drift-diffusion model including collisions. Preprint No. 923, WIAS Berlin, Germany, 2004.

[3] M. Baro, H.-C. Kaiser, H. Neidhardt, and J. Rehberg. A quantum transmitting Schrödinger-Poisson system. To appear in *Rev. Math. Phys.*, 2004.

[4] N. Ben Abdallah. A hybrid kinetic-quantum model for stationary electron transport in a resonant tunneling diode. *J. Stat. Phys.* 90 (1998), 627-662.

[5] N. Ben Abdallah, P. Degond, and I. Gamba. Coupling one-dimensional time-dependent classical and quantum transport models. *J. Math. Phys.* 43 (2002), 1-24.

[6] N. Ben Abdallah, F. Méhats, and N. Vauchelet. Analysis of a drift-diffusion-Schrödinger-Poisson model. *C. R. Acad. Sci. Paris, Ser. I* 335 (2002), 1007-1012.

[7] N. Ben Abdallah, O. Pinaud, C. Gardner, and C. Ringhofer. A comparison of resonant tunneling

based on Schrödinger's wquation and quantum hydrodynamics. VLSI Design 15 (2002), 695-700.

[8] B. Biegel. Simulation of ultra-small electronic devices: the classical-quantum transition regime. NASA Technical Report 97-028, 1997.

[9] Z. Chen, B. Cockburn, C. Gardner, and J. Jerome. Quantum hydrodynamic simulation of hysteresis in the resonant tunneling diode. *J. Comput. Phys.* 117 (1995), 274-280.

[10] P. Degond and A. El Ayyadi. A coupled drift-diffusion model for quantum semiconductor device simulations. *J. Comp. Phys.* 181 (2002), 222-259.

[11] P. Degond, F. Méhats, and C. Ringhofer. Quantum energy-transport and drift-diffusion models. Preprint, Université Paul Sabatier, Toulouse, France, 2003.

[12] P. Degond, F. Méhats, and C. Ringhofer. Quantum hydrodynamic models derived from the entropy principle. To appear in *Contemp. Math.*, 2004.

[13] P. Degond and C. Ringhofer. Quantum moment hydrodynamics and the entropy principle. *J. Stat. Phys.* 112 (2003), 587-628.

[14] C. de Falco, E. Gatti, A. Lacaita, and R. Sacco. Quantum-corrected drift-diffusion model for transport in semiconductor devices. Preprint, MOX, Politecnico di Milano, Italy, 2004.

[15] D. Ferry and J.-R. Zhou, *Form of the quantum potential for use in hydrodynamic equations for semiconductor device modeling*, *Phys. Rev. B* **48** (1993) 7944-7950.

[16] W. Frensley. Boundary conditions for open quantum systems driven far from equilibrium. *Rev. Modern Phys.* 62 (1990), 745-791.

[17] W. Frensley and N. Einspruch (eds.). *Heterostructures and Quantum Devices*. VLSI Electronics: Microstructure Science, Academic Press, San Diego, 1994.

[18] C. Gardner. The quantum hydrodynamic model for semiconductor devices. *SIAM J. Appl. Math.* 54 (1994), 409-427.

[19] K. Gullapalli, D. Miller, and D. Neilirk. Simulation of quantum transport in memory-switching double-barrier quantum-well diodes. *Phys. Rev. B* 49 (1994), 2622-2628.

[20] J. Höntschel, W. Klix, and R. Stenzel. Investigation of quantum transport phenomena in resonant tunneling structures by simulations with a novel quantum hydrodynamic transport model. *Proceedings of the 29th Internat. Symposium on Compound Semiconductors (ISCS)*, Lausanne, Switzerland, IoP Conference Series No. 174 (2002), 255-258.

[21] A. Jüngel. *Quasi-hydrodynamic Semiconductor Equations*. Birkhäuser, Basel, 2001.

[22] A. Jüngel and R. Pinnau. A positivity-preserving numerical scheme for a nonlinear fourth-order parabolic equation. *SIAM J. Num. Anal.* 39 (2001), 385-406.

[23] N. Kluksdahl, A. Kriman, D. Ferry, and C. Ringhofer. Self-consistent study of the resonant-tunneling diode. *Phys. Rev. B* 39 (1989), 7720-7735.

[24] C. Lent and D. Kirkner. The quantum transmitting boundary method. *J. Appl. Phys.* 67 (1990), 6353-6359.

[25] M. Lundstrom. *Fundamentals of Carrier Transport* (2nd edition). Cambridge University Press, Cambridge, 2000.

[26] O. Pinaud. Transient simulations of a resonant tuneling diode. *J. Appl. Phys.* 92 (2002), 1987-1994.

[27] T. Waho. Resonant tunneling diode and its application to multi-GHz analog-to-digital converters. *Proceedings of the seminar "Quantum Nanoelectronics for Meme-Media-Based Information Technologies"*, Sapporo, Japan (2003), 53-58.

[28] A. Wettstein. *Quantum effects in MOS devices*. PhD thesis, ETH Zürich, 2000.